Published in final edited form as:
NMR Biomed. 2008 November ; 21(10): 1094–1101. doi:10.1002/nbm.1286.

Diffusion tensor quantification of the macrostructure and microstructure of human midsagittal corpus callosum across the lifespan

Khader M. Hasan[1,*], **Linda Ewing-Cobbs**[2], **Larry A. Kramer**[1], **Jack M. Fletcher**[3], and **Ponnada A. Narayana**[1]

[1] Department of Diagnostic and Interventional Imaging, University of Texas Health Science Center Houston-Medical School, Houston, TX, USA

[2] Department of Pediatrics, University of Texas Health Science Center Houston-Medical School, Houston, TX, USA

[3] Department of Psychology, University of Houston, Houston, TX, USA

Abstract

The midsagittal cross-sectional area of the human corpus callosum (CC) has been used by many researchers as a marker of development, natural aging, and neurodegenerative and acquired pathologies. The availability of non-invasive MRI methods for quantifying the macrostructural and microstructural organization of the CC would help to clarify the CC contribution to behavior and cognition in both health and disease. In this report, we extended and validated the ability of a recently described semi-automated diffusion tensor imaging tissue segmentation method to utilize the high orientation contrast of the CC on diffusion tensor imaging. Using a cohort of healthy right-handed children and adults aged 7–59 years, we show gender-independent non-linear (quadratic) and strongly correlated growth trends in the CC area and the corresponding diffusion tensor fractional anisotropy ($r = 0.67$; $P < 1 \times 10^{-10}$). Our results provide preliminary evidence that diffusion tensor anisotropy in the living CC may be related to the number of small myelinated fibers.

Keywords

diffusion tensor imaging; corpus callosum; microstructure; macrostructure; healthy; children; adults; development; aging; lifespan

INTRODUCTION

The corpus callosum (CC) is the largest interhemispheric commissural white matter fiber network in the human brain (1,2). An estimated 200–300 million fibers of different myelination and axonal geometry cross the CC midline, yielding a cross-sectional area of ~200–1000 mm^2 during the lifespan (1–5). The CC has been used as a sensitive marker of brain hemispheric lateralization (2,6–7), connectivity and function (8–12), development (3,13–16), and natural aging (16–25). Different CC-derived measures, such as area (14,16,18–22), volume (26,27), thickness (11), shape (28), diffusion tensor regional

[*]Correspondence to: K. M. Hasan, Associate Professor of Diagnostic and Interventional Imaging, Department of Diagnostic and Interventional Imaging, University of Texas Medical School at Houston, 6431 Fannin Street, MSB 2.100, Houston, TX 77030, USA., khader.m.hasan@uth.tmc.edu.

anisotropy (12,23,24), principal diffusion eigenvector coherence (24), and fiber connectivity (10,25), have been used as neuroimaging markers in a host of developmental (26–31), neurodegenerative (32–34) and acquired pathologies (35–37). Because of a possible direct relation with the number of axons traversing the midline (2,5,8–10,31,32), the CC midsagittal area (CCA) has been the most commonly used measure in quantitative MRI and histological studies of the CC (2–9,16–22).

Both anatomical [conventional MRI (cMRI)] and quantitative methods such as relaxation, perfusion, magnetization transfer and diffusion tensor imaging (DTI) have provided important microstructural and macrostructural indices such as areas and anisotropy to assess the effect of developmental changes, injury, and disease on the CC. The availability of a single MRI modality to provide both microstructural and macrostructural attributes of the CC would significantly advance our knowledge about its role in health and disease.

The main goal of this work is to extend the utility of a DTI-based tissue segmentation methodology described recently (38) to the midsagittal CC. We applied this validated approach to a cohort of males and females aged 7–59 years to model the age effects of the CCA and corresponding DTI metrics. We show that the combination of the CCA (a macrostructural measure) and the corresponding DTI-derived metrics (microstructural indices) can be used to shed light on the contributors to *in vivo* MRI signal sources in the CC.

METHODS

Participants

This study included a total of 77 right-handed healthy children (n = 37; 19 boys/18 girls; mean ± SD age 11.0 ± 3.1 years) and adults (n = 40; 25 women/15 men; mean ± SD age 36.8 ± 12.2 years). The boys/girls, men/women, and male/female groups were age-matched ($P > 0.2$). All participants (age range 7–59 years; Table 1) were primarily English-speaking, identified as neurologically normal by review of medical history, and were healthy at the time of the assessments. The MRI scans were read as ‘normal’ by a board-certified radiologist (L.A.K.). Written informed consent from the adults, guardians, and adolescents, and assent from the children participating in these studies was obtained in accordance with our institutional review board regulations for the protection of human subjects.

MRI and DTI data acquisition and processing

These studies used a high signal-to-noise ratio whole-brain DTI protocol at 3.0 T, the duration of which was kept under 7 min (38,39). The diffusion-weighted data were collected axially (superior-to-inferior from the foramen magnum to the vertex) using 44 contiguous 3 mm sections that covered the entire brain. The diffusion sensitization or *b* factor = 1000 s/mm^2, and the encoding scheme used 21 uniformly distributed directions (39). In this work, the DTI-derived rotationally invariant metrics included the principal eigenvalue ($\lambda_{\|} = \lambda_1$), radial diffusivity [$\lambda_{\perp} = (\lambda_2 + \lambda_3)/2$], fractional anisotropy (FA) and mean diffusivity [$D_{\text{av}} = (\lambda_{\|} + 2 \times \lambda_{\perp})/3$]. Details of the DTI image processing and data quality control measures are provided elsewhere (40).

DTI-based segmentation of the CC

An experienced neurosurgeon assisted with midsagittal CC identification, which was based on the appearance of the inter-thalamic mass and the fornix on the isotropically interpolated DTI maps (33). The CC was then segmented on the midsagittal slice using mean diffusivity (D_{av}), FA and the principal eigenvector (38,41). The threshold selection for the CC was based on a feature space constructed from D_{av} versus FA of a large population of healthy

children and adults. The feature space was obtained using region-of-interest measurements placed on several locations on the midsagittal CC (see Fig. 1 in Ref. (38)).

Validation of the DTI-based midsagittal CCAs using manual delineation

The DTI-based CC segmentation was validated by manually delineating the CC on the midsagittal section using cMRI data acquired sagittally (Fig. 1a) immediately before the DTI data acquisition and in the same session. To account for variability in brain size (e.g. males versus females), we also manually delineated the forebrain cross-sectional area (FBA) on the midsagittal section to use it for CC normalization purposes as recommended by several studies (19,22,26,27). The forebrain delineation included the supratentorial–supracallosal midline area using the same sagittal section that was used to delineate the CC (Fig. 1a; see also figures in Refs (22) and (26)).

Statistical analysis

A Bland–Altman bias analysis of the difference versus mean was adopted to compare the manual and DTI-based CCA measurements (42). Analysis of variance was used to compare CCA mean values between groups (boys/girls, men/women, boys/men, girls/women, and males/females). All analyses of CCAs and the corresponding DTI metrics variation were conducted using a generalized linear model with effects of both age and sex. Given previous reports (16–21,43,44), both linear and quadratic age terms were included. Higher-order coefficient models (e.g. cubic) were not significantly better, as judged by goodness-of-fit statistical tests. The CCA, CCA/FBA and corresponding DTI metrics were modeled (fitted) for both males and females as: $y_f = \beta_0 + (\beta_1 \times \text{age}) + (\beta_2 \times \text{age}^2)$, then least-squares optimization methods were used to estimate the coefficients, standard deviations and their statistical significance using analysis of variance. For comparison of two fit parameters between males (M) and females (F), we used a two-tailed t test of the difference $(\beta_{iM} - \beta_{iF})$ divided by the root of the pooled variance $\sigma(\beta_{iM})^2 + \sigma(\beta_{iF})^2$ at the corresponding degrees of freedom (42). All statistical analyses were conducted using MATLAB R12.1 Statistical Toolbox v 3.0 (The Math-works Inc, Natick, MA, USA).

RESULTS

Validation of the semi-automated DTI CCA segmentation

Figure 1a shows a scatter plot and linear regression of the correspondence between the manual cMRI-based and DTI-based methods for the CCA measurements on the 34 males (19 boys/15 men) and 43 females (18 girls/25 women). Figure 2b shows the association between the CCA computed using the cMRI- and DTI-based methods on all children (n = 37) and adults (n = 40). Figure 2c shows the association of the two methods on boys, girls, men, and women. A strong correlation between the two methods using all possible age or gender stratifications is noted (Pearson correlation $r \sim 0.80$; $P < 0.00001$). A further bias analysis of the manual cMRI- and DTI-based methods using the Bland–Altman approach (42), which plots the mean of the two measurements against the difference (Fig. 1d), indicates that the DTI-based and cMRI measurements on the entire CCA have no significant bias or trend ($P > 0.5$).

Group mean comparisons between midsagittal and corresponding DTI metrics

Table 1 summarizes the mean ± SD results of the CCA and FBA and the normalized CCA/FBA × 100% on all subgroups of the entire sample: boys, girls, men, women, children, adults, males, females and all 77 participants. Table 2 summarizes the CC corresponding mean ± SD principal, radial, and mean diffusivities, and fractional anisotropy. The principal

eigenvalues were not significantly different between boys/girls, men/women, children/adults and males/females (analysis of variance, $P > 0.6$).

Age dependence of the macrostructure and microstructure attributes of the CC

Significant group differences between normalized callosal areas, D_{av}, radial diffusivity, and FA were noted between boys/men, girls/women, and children/adults (Tables 1 and 2). These exploratory results based on age subgroup mean value differences between boys/men, girls/women and children/adults underscore the importance of age in our study. The normalized CCA and its corresponding D_{av} and FA variation with age and sex are investigated in Fig. 2a, b, and c, respectively. Scatter plots corresponding to $\lambda_{||}$ and $\lambda_{\perp}$ are not shown. Note that $\lambda_{||}$ of the CCA is age- and gender-independent (Table 2), and, as $D_{av} = (\lambda_{||} + 2 \times \lambda_{\perp})/3$, and FA is a function of $(\lambda_{||}/\lambda_{\perp})$, then (i) D_{av} (age) ~$\lambda_{\perp}$(age), and (ii) FA (age)~ 1/[D_{av} (age)]. Note that our data as a function of age were best fitted with quadratic curves for both males and females. Table 3 summarizes the corresponding least-squares fit parameters for males and females separately, and the entire sample. There were no significant differences between males and females in the base-line (β_0), linear (β_1) and (β_2) quadratic coefficients of the best-fit parabolas ($P > 0.2$; Fig. 2a, b, c and Table 3).

Correlation between the macrostructural and microstructural measures of the CC

Figure 2d reveals a strong linear correlation between the normalized CCA (CCA/FBA) and the corresponding mean FA in the CC on all boys ($r = 0.67$; $P = 0.002$; $n = 19$), girls ($r = 0.51$; $P = 0.03$; $n = 18$), men ($r = 0.75$; $P = 0.001$; $n = 15$), women ($r = 0.50$; $P = 0.01$) and the entire cohort ($r = 0.66$; $P < 1 \times 10^{-10}$). The correlation and significance on the entire cohort between normalized CCA and mean, radial and principal diffusivities were $r = -0.58$ and $P < 2 \times 10^{-8}$, $r = -0.47$ and $P < 2 \times 10^{-5}$, and $r = -0.2$ and $P = 0.087$, respectively (scatter data not shown).

DISCUSSION

The CC is an ideal compact structure for studying white matter connectivity *in vivo* in both health and disease. The human midsagittal CC has been the focus of several MRI studies and a few postmortem histological studies on adults (5,31). It is commonly believed that the area of the CC may be related to the number and microstructure of the axons traversing the sagittal midline (1–14). To try to avoid controversial issues related to handedness (6,7), we selected a cohort of only right-handed healthy age-matched boys/girls and men/women. In this work, we selected the entire midsagittal section to help to standardize (9,19,22,28,30), validate and relate our work to previous quantitative reports. Future extensions of this work will examine issues related to callosal regional heterogeneity (26,27,33,37).

We validated the CC areas estimated with a semiautomated DTI-based segmentation method using manually delineated CCA and FBA on anatomical MRI data acquired in the sagittal plane. Our results on the gender-independent normalized callosal areas are consistent with previous MRI (14,18–21,31) and histological reports (5,31). The mean CCA, FBA, and CCA/FBA values, gender effects and non-linear age trends reported on both males and females are consistent with previous lifespan studies on the CC midsagittal cross-section (17–22). The U-shaped or parabolic growth curves of the normalized midsagittal CCA/FBA and corresponding FA are analogous to lifespan growth curves reported on white matter volume fraction in the entire brain (43,44). These non-linear brain white matter curves or ‘trajectories’ have been attributed to progressive myelination and axonal microstructural changes (16–21,38,43,44). Our results on the macrostructural and microstructural parabolic growth curves consolidate the CC measures in several cMRI and DTI studies on both healthy children (14–16,26) and adults (16–25,27).

This work reports in a healthy and right-handed cohort a strong correlation between the macrostructural (e.g. CCA/FBA) and microstructural (e.g. FA) attributes of the CC. Our results on both children and adults are consistent with two DTI studies that reported strong correlations between different CC volume measures and FA in both healthy children (26) and adults (27).

Contributors to CCA include axons with different myelin, size and shape distributions in addition to glia support cells. The contributors to DTI anisotropy in living and healthy white matter have not yet been resolved, even on compact structures such as the CC, internal capsule, and spinal cord (45,46). Diffusion anisotropy in white matter has been reported in unmyelinated structures (45,47) and has been attributed to several contributors, including axonal membranes (48), intravoxel coherence (49), intraxonal microstructure (50), myelination (51), and other biophysical factors [see Ref. (45) for an extensive review of the literature].

In this study, the principal eigenvalues were not significantly different between the age and gender subgroups in the entire cohort. The intravoxel coherence in the CC has been shown to be spatially uniform and similar between men and women (25), and hence it could not be the primary contributor to the measured CC anisotropy variation with age. On the basis of previous postmortem histological studies on adults (5,31), the CCA correlated with the number of small and lightly myelinated axons (fiber diameter ~0.4–1 μm) that are common across the CC (5,31). Without additional supporting MRI (10,52) and non-MRI data, we can only postulate that our results on the correlation between FA and CCA may imply that FA in the CC is related primarily to the number of these lightly myelinated axons.

The exact interpretation of the strong correspondence between CCA/FBA and DTI metrics such as FA on the axonal scale may require future CC regional histological studies and modeling using larger cohorts, which will be the focus of future endeavors. Our study presents normative baseline curves for the development and aging of both CCA and its corresponding DTI metrics. The strong relationship between CCA and FA may be useful for defining additional non-invasive neuroimaging markers for the study of brain white matter in both health and disease.

Acknowledgments

This work is funded by the American National Institutes of Health (NIH) Institute for Neurological Diseases and Stroke (NIH-NINDS: R01-NS052505-03) awarded to K.M.H., NIH-Child Health and Development (NICHD) R01-NS046308 awarded to L.E.C., and P01-HD35946 awarded to J.M.F. The purchase of the 3.0 T MRI clinical scanner was partially funded by NIH grant S10 RR19186 awarded to P.A.N. We thank Ambika Sankar, for assistance with data processing, and Vipul Kumar Patel, for helping with data acquisition.

Abbreviations used

CC	corpus callosum
CCA	corpus callosum midsagittal cross-sectional area
cMRI	conventional MRI
$\boldsymbol{D}_{\mathbf{av}}$	mean diffusivity
DTI	diffusion tensor imaging
FA	fractional anisotropy
FBA	midsagittal forebrain supratentorial–supracallosal area

References

1. Cook, ND. The Brain Code: Mechanisms of Information Transfer and the Role of the Corpus Callosum. Methuen; London: 1986.
2. Zaidel, E.; Iacoboni, M. The Parallel Brain: The Cognitive Neuroscience of the Corpus Callosum. MIT press; Cambridge: 2003.
3. Rakic P, Yakovlev PI. Development of the corpus callosum and cavum septi in man. J Comp Neurol 1968;132:45–72. [PubMed: 5293999]
4. De Lacoste MC, Kirkpatrick JB, Ross ED. Topography of the human corpus callosum. J Neuropathol Exp Neurol 1985;44:578–591. [PubMed: 4056827]
5. Aboitiz F, Scheibel AB, Fisher RS, Zaidel E. Fiber composition of the human corpus callosum. Brain Res 1992;598:143–153. [PubMed: 1486477]
6. Witelson SF, Goldsmith CH. The relationship of hand preference to anatomy of the corpus callosum in men. Brain Res 1991;545:175–182. [PubMed: 1860044]
7. Westerhausen R, Kreuder F, Dos Santos Sequeira S, Walter C, Woerner W, Wittling RA, Schweiger E, Wittling W. The association of macro- and microstructure of the corpus callosum and language lateralisation. Brain Lang 2006;97:80–90. [PubMed: 16157367]
8. Ringo JL, Doty RW, Demeter S, Simard PY. Time is of the essence: a conjecture that hemispheric specialization arises from interhemispheric conduction delay (Review). Cereb Cortex 1994;4:331–343. [PubMed: 7950307]
9. Steinmetz H, Staiger JF, Schlaug SG, Huang Y, Jäncke L. Inverse relationship between brain size and callosal connectivity. Naturwissenschaften 1996;83:221. [PubMed: 8668233]
10. Wahl M, Lauterbach-Soon B, Hattingen E, Jung P, Singer O, Volz S, Klein JC, Steinmetz H, Ziemann U. Human motor corpus callosum: topography, somatotopy, and link between microstructure and function. J Neurosci 2007;27:12132–12138. [PubMed: 17989279]
11. Luders E, Narr KL, Bilder RM, Thompson PM, Szeszko PR, Hamilton L, Toga AW. Positive correlations between corpus callosum thickness and intelligence. Neuroimage 2007;37:1457–1464. [PubMed: 17689267]
12. Bengtsson SL, Nagy Z, Skare S, Forsman L, Forssberg H, Ullén F. Extensive piano practicing has regionally specific effects on white matter development. Nat Neurosci 2005;8:1148–1150. [PubMed: 16116456]
13. LaMantia AS, Rakic P. Axon overproduction and elimination in the corpus callosum of the developing rhesus monkey. J Neurosci 1990;10:2156–2175. [PubMed: 2376772]
14. Giedd JN, Rumsey JM, Castellanos FX, Rajapakse JC, Kaysen D, Vaituzis AC, Vauss YC, Hamburger SD, Rapoport JL. A quantitative MRI study of the corpus callosum in children and adolescents. Brain Res Dev Brain Res 1996;91:274–280.
15. Snook L, Paulson LA, Roy D, Phillips L, Beaulieu C. Diffusion tensor imaging of neurodevelopment in children and young adults. NeuroImage 2005;26:1164–1173. [PubMed: 15961051]
16. Keshavan MS, Diwadkar VA, DeBellis M, Dick E, Kotwal R, Rosenberg DR, Sweeney JA, Minshew N, Pettegrew JW. Development of the corpus callosum in childhood, adolescence and early adulthood. Life Sci 2002;70:1909–1922. [PubMed: 12005176]
17. Hayakawa K, Konishi Y, Matsuda T, Kuriyama M, Konishi K, Yamashita K, Okumura R, Hamanaka D. Development and aging of brain midline structures: assessment with MR imaging. Radiology 1989;172:171–177. [PubMed: 2740500]
18. Pujol J, Vendrell P, Junque C, Marti-Vilalta JL, Capdevila A. When does human brain development end? Evidence of corpus callosum growth up to adulthood. Ann Neurol 1993;34:71–75. [PubMed: 8517683]
19. Rauch RA, Jinkins JR. Analysis of cross-sectional area measurements of the corpus callosum adjusted for brain size in male and female subjects from childhood to adulthood. Behav Brain Res 1994;64:65–78. [PubMed: 7840893]
20. Johnson SC, Farnworth T, Pinkston JB, Bigler ED, Blatter DD. Corpus callosum surface area across the human adult life span: effect of age and gender. Brain Res Bull 1994;35:373–377. [PubMed: 7850489]

21. McLaughlin NC, Paul RH, Grieve SM, Williams LM, Laidlaw D, Dicarlo M, Clark CR, Whelihan W, Cohen RA, Whitford TJ, Gordon E. Diffusion tensor imaging of the corpus callosum: a cross-sectional study across the lifespan. Int J Dev Neurosci 2007;25:215–221. [PubMed: 17524591]
22. Erdogan N, Ulger H, Tuna I, Okur A. A novel index to estimate the corpus callosum morphometry in adults: callosal/supratentorial-supracallosal area ratio. Diagn Interv Radiol 2005;11:179–181. [PubMed: 16320220]
23. Chepuri NB, Yen YF, Burdette JH, Li H, Moody DM, Maldjian JA. Diffusion anisotropy in the corpus callosum. AJNR Am J Neuroradiol 2002;23:803–808. [PubMed: 12006281]
24. Sullivan EV, Adalsteinsson E, Hedehus M, Ju C, Moseley M, Lim KO, Pfefferbaum A. Equivalent disruption of regional white matter microstructure in ageing healthy men and women. Neuroreport 2001;12:99–104. [PubMed: 11201100]
25. Ota M, Obata T, Akine Y, Ito H, Ikehira H, Asada T, Suhara T. Age-related degeneration of corpus callosum measured with diffusion tensor imaging. Neuroimage 2006;31:1445–1452. [PubMed: 16563802]
26. Alexander AL, Lee JE, Lazar M, Boudos R, DuBray MB, Oakes TR, Miller JN, Lu J, Jeong EK, McMahon WM, Bigler ED, Lainhart JE. Diffusion tensor imaging of the corpus callosum in Autism. Neuroimage 2007;34:61–73. [PubMed: 17023185]
27. Rotarska-Jagiela A, Schönmeyer R, Oertel V, Haenschel C, Vogeley K, Linden DE. The corpus callosum in schizophrenia: volume and connectivity changes affect specific regions. Neuroimage 2008;39:1522–1532. [PubMed: 18096406]
28. von Plessen K, Lundervold A, Duta N, Heiervang E, Klauschen F, Smievoll AI, Ersland L, Hugdahl K. Less developed corpus callosum in dyslexic subjects: a structural MRI study. Neuropsychologia 2002;40:1035–1044. [PubMed: 11900755]
29. Barkovich AJ, Norman D. Anomalies of the corpus callosum: correlation with further anomalies of the brain. AJNR Am J Neuroradiol 1988;151:71–79.
30. Laissy JP, Patrux B, Duchateau C, Hannequin D, Hugonet P, Ait-Yahia H, Thiebot J. Midsagittal MR measurements of the corpus callosum in healthy subjects and diseased patients: a prospective study. AJNR Am J Neuroradiol 1993;14:145–154. [PubMed: 8427077]
31. Highley JR, Esiri MM, McDonald B, Cortina-Borja M, Herron BM, Crow TJ. The size and fibre composition of the corpus callosum with respect to gender and schizophrenia: a post-mortem study. Brain 1999;122:99–110. [PubMed: 10050898]
32. Evangelou N, Konz D, Esiri MM, Smith S, Palace J, Matthews PM. Regional axonal loss in the corpus callosum correlates with cerebral white matter lesion volume and distribution in multiple sclerosis. Brain 2000;123:1845–1849. [PubMed: 10960048]
33. Hasan KM, Gupta RK, Santos RM, Wolinsky JS, Narayana PA. Fractional diffusion tensor anisotropy of the seven segments of the normal-appearing white matter of the corpus callosum in healthy adults and relapsing remitting multiple sclerosis. J Magn Reson Imaging 2005;21:735–743. [PubMed: 15906348]
34. Wiltshire K, Foster S, Kaye JA, Small BJ, Camicioli R. Corpus callosum in neurodegenerative diseases: findings in Parkinson's disease. Dement Geriatr Cogn Disord 2005;20:345–351. [PubMed: 16192724]
35. Gupta RK, Saksena S, Hasan KM, Agarwal A, Haris M, Pandey CM, Narayana PA. Focal Wallerian degeneration of the corpus callosum in large middle cerebral artery stroke: serial diffusion tensor imaging. J Magn Reson Imaging 2006;24:549–555. [PubMed: 16888796]
36. Ewing-Cobbs L, Hasan KM, Prasad MR, Kramer L, Bachevalier J. Corpus callosum diffusion anisotropy correlates with neuropsychological outcomes in twins disconcordant for traumatic brain injury. AJNR Am J Neuroradiol 2006;27:879–881. [PubMed: 16611782]
37. Moeller FG, Hasan KM, Steinberg JL, Kramer LA, Dougherty DM, Santos RM, Valdes I, Swann AC, Barratt ES, Narayana PA. Reduced anterior corpus callosum white matter integrity is related to increased impulsivity and reduced discriminability in cocaine-dependent subjects: diffusion tensor imaging. Neuropsychopharmacology 2005;30:610–617. [PubMed: 15637640]
38. Hasan KM, Halphen C, Sankar A, Eluvathingal TJ, Kramer L, Stuebing KK, Ewing-Cobbs L, Fletcher JM. Diffusion tensor imaging-based tissue segmentation: validation and application to the developing child and adolescent brain. Neuroimage 2007;34:1497–1505. [PubMed: 17166746]

39. Hasan KM, Halphen C, Boska MD, Narayana PA. Diffusion tensor metrics, T2 relaxation, and volumetry of the naturally aging human caudate nuclei in healthy young and middle-aged adults: possible implications for the neurobiology of human brain aging and disease. Magn Reson Med 2008;59:7–13. [PubMed: 18050345]
40. Hasan KM. A framework for quality control and parameter optimization in diffusion tensor imaging: theoretical analysis and validation. Magn Reson Imaging 2007;25:96–112.
41. Kanabar, BP.; Hasan, KM.; Sajja, BR.; Narayana, PA. A diffusion tensor imaging based semi-automated segmentation and subdivision of the human corpus callosum: correlation of anisotropy and callosal area and application to gender based differences. Proceedings of the 13th Annual Meeting ISMRM; Miami, USA. p. 1347
42. Glantz, SA. Primer of Biostatistics. 5. McGraw-Hill; New York: 2002.
43. Sowell ER, Peterson BS, Thompson PM, Welcome SE, Henkenius AL, Toga AW. Mapping cortical change across the human life span. Nat Neurosci 2003;6:309–315. [PubMed: 12548289]
44. Hasan KM, Sankar A, Halphen C, Kramer LA, Brandt ME, Juranek J, Cirino PT, Fletcher JM, Papanicolaou AC, Ewing-Cobbs L. Development and organization of the human brain tissue compartments across the lifespan using diffusion tensor imaging. Neuroreport 2007;18:1735–1739. [PubMed: 17921878]
45. Beaulieu C. The basis of anisotropic water diffusion in the nervous system: a technical review. NMR Biomed 2002;15:435–455. [PubMed: 12489094]
46. Pierpaoli C, Jezzard P, Basser PJ, Barnett A, Di Chiro G. Diffusion tensor MR imaging of the human brain. Radiology 1996;201:637–648. [PubMed: 8939209]
47. Wimberger DM, Roberts TP, Barkovich AJ, Prayer LM, Moseley ME, Kucharczyk J. Identification of “premyelination” by diffusion-weighted MRI. J Comput Assist Tomogr 1995;19:28–33. [PubMed: 7529780]
48. Takahashi M, Hackney DB, Zhang G, Wehrli SL, Wright AC, O’Brien WT, Uematsu H, Wehrli FW, Selzer ME. Magnetic resonance microimaging of intraaxonal water diffusion in live excised lamprey spinal cord. Proc Natl Acad Sci USA 2002;99:16192–16196. [PubMed: 12451179]
49. Takahashi M, Ono J, Harada K, Maeda M, Hackney DB. Diffusional anisotropy in cranial nerves with maturation: quantitative evaluation with diffusion MR imaging in rats. Radiology 2000;216:881–885. [PubMed: 10966726]
50. Kinoshita Y, Ohnishi A, Kohshi K, Yokota A. Apparent diffusion coefficient on rat brain and nerves intoxicated with methylmercury. Environ Res 1999;80:348–354. [PubMed: 10330308]
51. Song SK, Yoshino J, Le TQ, Lin SJ, Sun SW, Cross AH, Armstrong RC. Demyelination increases radial diffusivity in corpus callosum of mouse brain. Neuroimage 2005;26:132–140. [PubMed: 15862213]
52. Cader S, Johansen-Berg H, Wylezinska M, Palace J, Behrens TE, Smith S, Matthews PM. Discordant white matter N-acetylasparate and diffusion MRI measures suggest that chronic metabolic dysfunction contributes to axonal pathology in multiple sclerosis. Neuroimage 2007;36:19–27. [PubMed: 17398118]

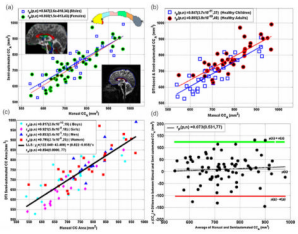

Figure 1.
Scatter plot of cMRI-measured versus DTI-measured CCA (mm^2) of (a) males versus females, (b) children versus adults and (c) boys/girls, men/women, and (d) a Bland–Altman analysis of the mean versus the difference of the two methods, indicating strong correspondence with minimal bias. The inserts in (a) on the horizontal and vertical axes represent the cMRI and DTI-based callosal delineation (segmentation) methods, respectively.

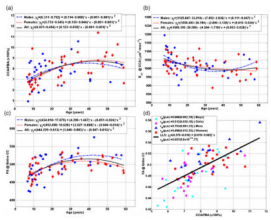

Figure 2.

Representative scatter data and quadratic least-squares fit of the growth curves for males (boys and men; n = 34), females (girls and women; n = 43) and the entire sample (n = 77) corresponding to (a) CCA/FBA, (b) D_{av} and (c) FA as function of age, and (d) a scatter plot of and linear regression of the correspondence between the CCA/FBA and FA (Tables 1–3). Scatter plots corresponding to $\lambda_{||}$ and $\lambda_{\perp}$ are not shown. Note that $\lambda_{||}$ of the CCA is age-and gender-independent (Table 2), and, as $D_{av} = (\lambda_{||} + 2 \times \lambda_{\perp})/3$, and FA is a function of $(\lambda_{||}/\lambda_{\perp})$, then (i) D_{av} (age) ~$\lambda_{\perp}$(age), and (ii) FA(age) ~1/[D_{av}(age)].

Table 1

Age, CCA, FBA, and normalized callosal area (CCA/FBA × 100%) of the healthy right-handed control boys, girls, men, women, children, adults, males, and females in this study (mean ± SD)

Group	No.	Age	CCA (mm^2)	FBA (mm^2)	CCA/FBA × 100%
Boys	19	11.4 ± 3.2	710.4 ± 96.6	9584.6 ± 747.2	7.5 ± 1.2
Girls	18	10.5 ± 2.9	653.8 ± 85.6	9323.2 ± 573.2	7.0 ± 1.0
Children	37	11.0 ± 3.1	682.9 ± 94.6	9457.4 ± 672.2	7.3 ± 1.1
Men	15	35.6 ± 12.0	791.2 ± 82.4	9737.5 ± 1044.3	8.2 ± 1.5
Women	25	37.6 ± 12.5	772.4 ± 93.0	9182.4 ± 850.4	8.5 ± 1.1
Adults	40	36.8 ± 12.2	779.4 ± 88.6	9390.5 ± 954.2	8.4 ± 1.3
Males	34	22.1 ± 14.7	746.1 ± 98.1	9652.0 ± 879.3	7.8 ± 1.4
Females	43	26.2 ± 16.6	722.7 ± 106.8	9241.3 ± 742.4	7.9 ± 1.3
All	77	24.4 ± 15.8	733.0 ± 103.1	9422.7 ± 826.1	7.8 ± 1.3

Table 2

Basic principal, radial and mean diffusivity and fractional anisotropy in the CCA for healthy right-handed control boys, girls, men, women, children, adults, males, and females in this study (mean ± SD)

Group	$\lambda_{\perp}$ ($\times 10^{-6}$ mm^2/s)	$\lambda_{\parallel}$ ($\times 10^{-6}$ mm^2/s)	D_{av} ($\times 10^{-6}$ mm^2/s)	FA ($\times 1000$)
Boys	728.7 ± 73.2	1675.0 ± 89.4	1044.1 ± 72.5	480.0 ± 35.6
Girls	719.4 ± 37.0	1661.2 ± 79.0	1033.3 ± 44.5	480.6 ± 23.5
Children	724.2 ± 57.9	1668.3 ± 83.7	1038.9 ± 59.9	480.3 ± 29.9
Men	675.8 ± 38.9	1667.1 ± 56.9	1006.3 ± 38.0	513.1 ± 26.1
Women	683.4 ± 47.6	1644.5 ± 77.3	1003.8 ± 54.6	502.4 ± 19.3
Adults	680.6 ± 44.1	1653.0 ± 70.4	1004.7 ± 48.5	506.4 ± 22.4
Males	705.4 ± 65.4	1671.5 ± 75.9	1027.4 ± 62.0	494.6 ± 35.5
Females	698.5 ± 46.6	1651.5 ± 77.5	1016.1 ± 52.2	493.3 ± 23.5
All	701.5 ± 55.4	1660.3 ± 77.0	1021.1 ± 56.6	493.9 ± 29.2

NMR Biomed. Author manuscript; available in PMC 2011 February 28.

Table 3

Corpus callosum midsagittal macrostructural (CCA, CCA/FBA) and microstructural (FA, $\lambda_\perp$ and D_{av}) versus age quadratic least-squares fit parameters and statistics: $y = \beta_0 + (\beta_1 \times age) + (\beta_2 \times age^2) + \eta$

Metric	Group[a]	R^2	β_0 ± SD (P)	β_1 ± SD (P)	β_2 ± SD (P)
CCA (mm^2)	M	0.301	599.7 ± 50.5 (P*)[b]	10.6 ± 4.3 (0.02)	−0.126 ± 0.072 (0.091)
	F	0.409	516.8 ± 44.5 (P*)	14.7 ± 3.6 (0.0001)	−0.188 ± 0.058 (0.001)
	M & F	0.341	555.1 ± 33.5 (P*)	13.0 ± 2.8 (P*)	−0.164 ± 0.045 (0.001)
	M vs F (P)		0.22	0.47	0.50
CCA/FBA (×100%)	M	0.139	6.31 ± 0.79 (P*)	0.11 ± 0.07 (0.11)	−0.001 ± 0.001 (0.21)
	F	0.398	5.73 ± 0.55 (P*)	0.14 ± 0.04 (0.004)	−0.001 ± 0.001 (0.04)
	M & F	0.262	6.02 ± 0.46 (P*)	0.12 ± 0.04 (0.002)	−0.001 ± 0.001 (0.03)
	M vs F		0.55	0.79	0.98
D_{av} ($\times 10^{-6}$ mm^2/s)	M	0.253	1125.8 ± 33.0 (P*)	−7.95 ± 2.84 (0.009)	0.111 ± 0.047 (0.025)
	F	0.142	1056.5 ± 26.2 (P*)	−2.09 ± 2.14 (0.33)	0.015 ± 0.034 (0.66)
	M & F	0.174	1086.2 ± 20.6 (P*)	−4.50 ± 1.72 (0.01)	0.053 ± 0.028 (0.06)
	M vs F		0.10	0.10	0.10
$\lambda_\perp$ ($\times 10^{-6}$ mm^2/s)	M	0.354	822.0 ± 32.4 (P*)	−9.03 ± 2.78 (0.003)	0.119 ± 0.046 (0.015)
	F	0.224	755.7 ± 22.2 (P*)	−3.62 ± 1.82 (0.05)	0.039 ± 0.029 (0.18)
	M & F	0.275	784.8 ± 18.9 (P*)	−5.93 ± 1.58 (P*)	0.073 ± 0.026 (0.006)
	M vs F		0.10	0.11	0.15
FA (×1000)	M	0.391	434.9 ± 17.1 (P*)	4.30 ± 1.47 (0.006)	−0.051 ± 0.024 (0.047)
	F	0.306	452.5 ± 10.6 (P*)	3.03 ± 0.87 (0.001)	−0.040 ± 0.014 (0.006)
	M & F	0.324	444.2 ± 9.6 (P*)	3. 65 ± 0.80 (P*)	−0.047 ± 0.013 (0.001)
	M vs F		0.38	0.46	0.72

[a] M, males; F, females.

[b] P*< 0.000001.

The principal diffusivity ($\lambda_{||}$) did not change significantly with age [both linear (β_1) and quadratic (β_2) coefficients were not statistically significant; P > 0.6].